Journal of Radiation and Nuclear Applications
An International Journal

http://dx.doi.org/10.18576/jrna/110111

Accumulation and Leaching Zones of Uranium Specification by Radionuclides Mobility in Al-Madinah Al-Munawarah Soils Following Intense Rainfall Events

Zainab Z. Alfull[1] and Mahmoud R. Khatab[23]*

[1]Physics Department, Taibah University, El Madina El Munawarah, Saudi Arabia.
[2]Department of Mechanical and Nuclear Engineering, Virginia Commonwealth University, 401 West Main Street, Richmond, Virginia 23284.
[3]Geochemical Exploration Department, Research Sector, Nuclear Materials Authority, P.O. Box 530, El-Maadi, Cairo, Egypt.

Received: 30 Aug. 2025, Revised: 20 Oct. 2025, Accepted: 30 Nov. 2025
Published online: 1 Jan. 2026

Abstract: Al-Madinah is located in the western province of the Kingdom of Saudi Arabia, approximately 150 km east of the Red Sea and around 400 km north of Makkah, encircled by mountains composed of volcanic and magnetic plutonic rocks. Soil samples gathered from the vicinity of Al-Madinah Al-Munawarah were analyzed radiometrically utilizing an HPGe detector. The activity concentrations of ^{238}U ranged from 9.6±0.1 to 15.4±0.6 Bq.kg^{-1}, while ^{232}Th varied between 6.3±0.5 and 7.9±0.4 Bq.kg^{-1}, ^{226}Ra was found between 6.2±0.6 and 8.3±0.4 Bq.kg^{-1}, and 40K levels ranged from 169.3±2.3 to 343.5±1.8 Bq.kg^{-1}. The radionuclide concentrations in the examined soil are below international thresholds, indicating that their application is safe. Our findings revealed that the Th/U ratio in the soils and bottom sediments is less than 3.5, indicating uranium enrichment. The ratios of ^{234}U/^{238}U and ^{230}Th/^{238}U suggested that the majority of soil samples were situated within the accumulation zone, except for two samples found in the restricted zone, indicating turbid conditions. The ^{234}U/^{238}U activity ratio in most soil samples exceeded unity, ranging from 1.22±0.09 to 1.83±0.15, with one sample showing a value below 1; specifically, 0.93±0.06, which indicates relatively recent uranium uptake and preferential accumulation of ^{234}U due to prevailing reducing conditions; that is, less than 1 million years from fluids that transported excess ^{234}U from nearby rocks. The variation in the ^{230}Th/^{234}U activity ratio may be attributed to differences in the chemical characteristics of uranium and thorium, along with α-decay enhanced dissolution, re-adsorption, and re-precipitation of ^{234}U. All calculated environmental hazard parameters for the soil samples fall within the range of international standards, affirming their safe use. The cluster analysis indicates that the primary environmental health hazard parameters arise from the activity concentrations of ^{238}U and ^{226}Ra.

Keywords: Environment; Mobilization; Soil; Torrential Rains; Saudi Arabia.

1 Introduction

It is essential to thoroughly understand the distribution and concentration of terrestrial isotopes to monitor the environmental impact of natural radioactivity. In recent decades, researchers have conducted extensive studies across various countries to investigate the effects of terrestrial gamma radiation on human health. The primary objectives of these investigations were to establish global benchmark data that would enable us to monitor any future changes in environmental radioactivity resulting from factors such as nuclear energy, industrial activities, and other anthropogenic influences [1]. Additionally, the studies aimed to assess the levels of radiation exposure experienced by individuals in the examined regions. The natural radioactivity we encounter and the gamma radiation present in outdoor environments are primarily attributed to the concentration of radionuclides found in the Earth's soil [2]. Given that the majority of human radiation exposure originates from natural sources, the extent of ionizing radiation exposure has become a significant area of interest. Naturally occurring radionuclides can be detected in various environmental components, including soil, sediment, water, vegetation, and even the atmosphere [3].

*Corresponding author e-mail:

The distribution patterns of uranium and thorium have proven to be highly beneficial in studies related to environmental science, marine science, and geology. This is due to their critical role in tracing the movement of uranium series radionuclides and groundwater as it traverses different aquifer systems [4].

Natural radioactivity in soils mainly originates from isotopes like ^{238}U, ^{232}Th, and ^{40}K, as well as other elements within their radioactive decay series. Consistent monitoring of soil radioactivity is crucial for identifying any changes in activity over time due to radioactive emissions. To ensure effective radiological safety, it is vital to observe the discharge of radiation into the environment [5].

The primary sources of external gamma radiation exposure from natural origins include ^{238}U, ^{226}Ra, ^{232}Th, and 40K. Due to the non-uniform distribution of these radionuclides and their decay products in soil and sand, it is crucial to comprehend their presence and that of their progeny for effective radiation monitoring and safety measures. Assessing the individual contribution of each source to the overall radiation dose received is essential **[**6**]**. Uranium and thorium are typically present in a majority of minerals, with average concentrations in the Earth's crust estimated at ~ 2 ppm for uranium and 12 ppm for thorium. A significant feature of uranium is its propensity to oxidize easily and transform into uranyl (U^{6+}), setting it apart from other elements. This hexavalent form of uranium can create compounds through reactions with oxygen and complex molecules such as carbonates, sulfates, and fluorides. Furthermore, it has the potential to precipitate in rocks that contain materials conducive to reduction [7].

The background radiation originating from the natural environment is largely influenced by the specific geological and geographical characteristics of a given location, with the composition of rocks being particularly crucial. Igneous rocks, such as granite, typically display higher radiation levels in comparison to sedimentary rocks, which usually exhibit lower levels. However, certain varieties of shale and phosphate rocks can contain a significant concentration of radionuclides. The main sources of natural radionuclides arise from the decay chains of three isotopes: ^{235}U, ^{238}U, and ^{232}Th, in addition to ^{40}K. Among these, the isotope with the longest half-life is ^{232}Th, which persists for 1.405×10^{10} years, followed by ^{238}U, which has a half-life of 4.47×10^{9} years. The natural isotopic composition of uranium by mass is approximately 99.2745 % 238U, 0.72 % ^{235}U, and 0.0055 % ^{234}U [8].

El Galy et al., 2008 [9] stated that a disequilibrium exists between the radionuclides of the ^{238}U and ^{232}Th series, specifically before and after ^{226}Ra and ^{228}Ra, respectively. This disequilibrium arises from the differences in the chemical and physical characteristics of the various elements within the radioactive series, and weathering processes may lead to the migration of certain radionuclides.

Adagunodo et al. (2019 10) evaluated the radiological risks linked to farmers' exposure to radionuclides, and they investigated the distribution of radioactivity concentrations of ^{238}U, ^{232}Th, and ^{40}K in soil samples that were randomly collected from ten agricultural sites in Odo Oba, located in southwest Nigeria. The average concentrations of ^{238}U, ^{232}Th, and ^{40}K were found to be 29.40, 44.25, and 1072.04 Bq kg^{-1}, respectively.

Furthermore, the samples emit ^{222}Rn and ^{220}Rn, and the recoil of the residual nuclei after disintegration by alpha and/or beta particles may result in the deterioration of the crystal structure. The radioactive equilibrium of the isotopes ^{238}U, ^{234}U, and ^{230}Th is established in closed geological systems after 1.7 million years, at which point their corresponding activity ratios of ^{234}U/^{238}U, ^{230}Th/^{234}U, and ^{230}Th/^{238}U all reach unity. The varying physico-chemical conditions impacting ^{238}U and ^{234}U can lead to fractionation if the systems are subjected to weathering and groundwater flow, producing activity ratios that deviate from unity. Uranium isotopic signatures can be utilized to track the reductive remediation of subsurface contamination or to reconstruct paleo-redox environments [11].

Abuelnaga et al., 2021 [12] examined Al Madinah Al Monawarah, Saudi Arabia, utilizing a radiation car-borne scanner to evaluate the risks associated with radiation dose rates. The findings revealed that the average radiation dose in the studied area is 1.08 mSv y^{-1}, with values ranging from 0.001 to 4.41 mSv y^{-1}. In the Al Aziziah area and its vicinity, the estimated effective doses exceeded the public exposure limit of 1 mSv y^{-1}, yet remained below the occupational exposure threshold of 20 mSv y^{-1}. In this locality, granitic rocks present an average dose rate of approximately 2.4 mSv y^{-1}, while the deposits of these rocks yield an average dose rate of 1.2 mSv y^{-1}. A lower average dose is observed in basalt, basaltic, and basic deposits. However, further investigation is necessary to determine the radon levels in enclosed environments. The uranium contour and radiation dose maps reveal that radiation doses exceed permissible levels at locations near artificial drainage canals, making the accumulated water that flows into the wells unsuitable for drinking. There is an urgent need to enhance awareness regarding the environmental conditions in which communities live, especially in granite regions where radon may accumulate in confined spaces, potentially posing health risks.

This work aims to indicate the distribution of different radionuclides, their migration and accumulation in the soil of Al-Madinah Al-Munawarah after heavy torrential rains, and assess the possible radiological health hazards by comparing their results with the international levels.

2 Materials and methods

2.1. Gamma Ray Spectrometry

A total of ten soil samples were collected from representative sites throughout the Al-Madinah Al-Munawarah region to reflect the variability in land use and geomorphological conditions. The sampling locations comprised urban soils, agricultural fields, wadi beds, and regions characterized by granitic outcrops that may be enriched in uranium and thorium. At each location, surface soil was collected from the upper 0-5 cm using a stainless-steel auger, adhering to a five-point composite sampling method within a 10 m x 10 m grid to reduce spatial heterogeneity. The samples were placed in pre-cleaned polyethylene bags, labeled with GPS coordinates and depth, and transported to the laboratory in cool, sealed containers to prevent cross-contamination or moisture loss. All samples underwent air-drying, homogenization, sieving (< 2 mm), and were stored in airtight containers for future gamma spectrometric and geochemical analyses.

In order to prevent contamination of the spectrometer and the release of ^{222}Rn and ^{220}Rn radiogenic gases, which facilitate the attainment of radioactive secular equilibrium within the decay chains, the sample containers were securely sealed and stored for a minimum duration of four weeks **[**13**]**. The samples were analyzed using a Hyper Pure Germanium (HPGe) gamma-ray detector with a relative efficiency of 60 %. By employing efficiency-specific radionuclide methodologies and accounting for self-absorption effects of the gamma photon-emitting source, the uncertainty associated with gamma-ray intensities was effectively reduced **[**14**]**. The gamma lines corresponding to its daughter isotopes, 63.3 keV and 1001 keV for ^{234}Th and ^{234m}Pa, respectively, indicated the observed activity concentrations of ^{238}U **[**15**]**. The activity concentration of ^{234}U was directly computed from the gamma lines at 53.2 keV and 120.9 keV **[**16**]**. The gamma lines of ^{228}Ac at 338.4 keV and 911.2 keV, along with the gamma lines of ^{208}Tl, were utilized to determine the specific activity concentration of ^{232}Th at 583 keV and 2614.4 keV. The average activity of ^{226}Ra's daughter isotopes, ^{220}Rn, ^{214}Pb, and ^{214}Bi, was employed to calculate its activity concentration [17].

The activity concentration of ^{40}K was directly measured through its γ-line at 1460.8 keV. The overall uncertainty in the calculated activity concentrations is frequently below 10 %. Both ^{214}Bi and 214Pb emit detectable gamma rays, and either can be utilized to indirectly ascertain ^{226}Ra, which is a precursor in the decay chain that produces lead and bismuth progeny. The activity concentration of 214Pb was determined using the γ-lines at 241.9, 295.2, and 351.9 keV, while the activity concentrations of ^{214}Bi and ^{210}Pb were assessed using the γ-lines at 609.3 and 46.5 keV, respectively **[**16**]**. The γ-lines at 143.8 keV, 10.5 %, 163.4 keV, 4.8 %, and 205.3 keV were employed to evaluate the activity concentrations of ^{235}U, 4.7 %. The region of the peak at the next most likely energy, 143.76 keV, was utilized to calculate the ^{235}U activity concentration, which was found to be 10.96 %. The area corresponding to the 185.72 keV; 57.2 % ^{235}U peak was subsequently computed using the ratio of the gamma-branching ray, efficiency, and activity. The area attributed to ^{226}Ra was determined by subtracting the 235U peak from the peak area at 186 keV **[**18**]**.

The energy calibration was done using standard point sources ^{133}Ba, ^{137}Cs, and ^{60}Co, which have gamma-ray energies of 0.356, 0.662, 1.17, and 1.33 MeV, respectively. The efficiency calibration was performed, which contains both ^{226}Ra, 732 Bq kg^{-1}, and ^{232}Th, 17.8 ppm. To calculate the activity concentrations, Eq. (1) for ^{238}U, ^{226}Ra, ^{232}Th, and ^{40}K has been used.

$$\mathbf{A= Np/P\gamma.\ \eta.\ m \quad (1)}$$

where Np is the net counts per second, Pγ is the absolute transition probability of gamma decay, η is the detector efficiency, and m is the sample mass in kg. For quality assurance, the uncertainty of activity UA was calculated by Eq. 2 [19].

$$\mathbf{UA = A\sqrt{[U(Np)/Np]2+[u(\eta)/\eta]2+[u(m)/m]2+[u(P\gamma)/P\gamma]2 \quad (2)}}$$

2.2. Calculation of Environmental Hazard Parameters

2.2.1. Radium Equivalent Activity (Ra_{eq})

It is a useful index for comparing the individual activity of samples with varying quantities of ^{238}U, ^{232}Th, and ^{40}K. Around the world, granitic rocks and other raw materials are utilized in construction, and their corresponding natural radioactivity levels are mostly determined by the amount of their radioisotopes (^{238}U, ^{226}Ra, ^{232}Th, and ^{40}K).

The radium equivalent activity index, Raeq, is one of the indices used to evaluate the gamma radiation risks emitted by these radioisotopes. The Ra_{eq} index, which is a weighted sum of the specific activities of radioisotopes (^{226}Ra, ^{232}Th, and ^{40}K), expresses the specific activities of ^{238}U, ^{232}Th, and ^{40}K by a single quantity by assuming that 370 Bq kg^{-1} of ^{226}Ra, 259 Bq kg^{-1} of ^{232}Th, and 4810 Bq kg^{-1} of ^{40}K yield the same gamma dose rate. Ra_{eq} can be calculated from the following equation [20];

$$\mathbf{Raeq= A_U + 1.43\ A_{Th} + 0.077\ A_K \quad (3)}$$

2.2.2. Absorbed Gamma Dose Rate (AGDR)

Because the radiological and clinical effects are closely related to the absorbed dose rate, calculating the absorbed dose rate is the first important step in evaluating the potential health risk. To convert the measured activity concentrations of ^{226}Ra, ^{232}Th, and ^{40}K into doses, the conversion factors 0.462, 0.604, and 0.042 are employed, respectively [21]. These factors are used to calculate the absorbed gamma dose rate (AGDR) in nGy h^{-1} using the following equation;

$$\mathbf{AGDR = 0.462\ A_{Ra} + 0.604\ A_{Th} + 0.042\ A_K} \quad (4)$$

Where C_{Ra}, C_{Th}, and C_K are the activity concentrations (Bq kg^{-1}) of ^{226}Ra, ^{232}Th, and ^{40}K. The world average dose rate must be lower than 55 nGy.h^{-1} **[**22**]**.

2.2.3. Annual Effective Dose Rate

The effective dose equivalent is calculated using the measured value of the absorbed dose rate in the air. The conversion coefficient from the absorbed dose rate in the air to the effective dose equivalent received by an adult must be considered to verify these results [23]. The values of these two variables vary depending on the population's average age and the area's climate. To estimate the annual effective dose rates, the conversion coefficient from absorbed dose in air to effective dose, 0.7 Sv $Gy^{-1,}$ and the outdoor occupancy factor, 0.2 [15]. The following equation is used for the determination of the Annual Effective Dose Rate;

$$\mathbf{AEDR\ (mSv\ yr^{-1}) = ADR\ (nGy\ h^{-1}) \times 8760\ hyr^{-1} \times 0.7 \times (10^3 mSv/10^9)\ nGy \times 0.2 = D\ (mSv\ y^{-1}) \times 1.23 \times 10^{-3}} \quad (5)$$

2.2.4. External Hazard and Internal Hazard (H_{ex} and H_{in})

The emitted gamma radiation's external hazard index (H_{ex}) is used to evaluate the external hazard. The following equation is used to calculate it **[**24**];**

$$\mathbf{H_{ex} = CRa/370 + CTh/259 + CK/4810} \quad (6)$$

where H_{ex} is the external hazard index and C_{Th}, C_{Ra}, and C_K are the activities of ^{232}Th, ^{226}Ra, and ^{40}K in Bq kg^{-1}, respectively.

The upper limit of this index is 1. Internal exposure to ^{222}Rn and its radioactive progeny is controlled using the internal hazard index (H_{in}). It can be calculated using the equation below.

$$\mathbf{H_{in} = C_{Ra}/185 + C_{Th}/259 + C_K/4810} \quad (7)$$

2.2.5. Gamma Index (I_γ)

The γ-radiation level index is performed as a scanning tool to identify materials that could become of health interest when used as building materials. The value of the γ-index must be less than unity to keep the radiation risk to a minimum, and the radiation exposure from construction materials due to radioactivity must be limited to 1.5 mSv y^{-1}. By using the following equation, the γ-index is calculated [25]

$$\mathbf{I_\gamma = C_{Ra}/150 + C_{Th}/100 + C_K/1500} \quad (8)$$

2.2.6. Excess Lifetime Cancer Risk (ELCR)

The excess lifetime cancer risk (ELCR) is a radiological indicator used to estimate the probability of individuals having cancer due to continuous exposure to a substance. From the results of the annual effective dose at a given exposure level, we can determine the probability of contracting cancer. It's defined as a number representing the number of increased cancers that can be expected in a given number of people exposed to a carcinogen at a given dose and calculated from the following equation [24];

$$\mathbf{ELCR = AED \times DL \times RF} \quad (9)$$

Where AED is the Annual Equivalent Dose, DL is the average duration of life evaluated to be 70 years, and RF is the risk factor; Sv^{-1}, i.e., fatal cancer risk per Sievert.

2.2.7. Annual Gonadal Dose Equivalent

A measure of the genetic significance of the yearly dose equivalent received by the population's reproductive organs (gonads) is the annual gonadal dose equivalent (AGDE). In the same context, the activity of bone marrow and the bone surface cells is considered the organ of interest. Therefore, the annual gonadal dose equivalent due to the specific activities of ^{238}U, ^{232}Th, and ^{40}K is computed using the following expression **[**26**]**;

$$\mathbf{AGDE\ (mSv\ y^{-1}) = 3.09\ A_{Ra} + 4.18\ A_{Th} + 0.314\ A_K} \quad (10)$$

2.3. Geological Setting

Al-Madinah is located in the western part of the Arabian Peninsula, known as the Arabian Shield, which comprises predominantly Precambrian crystalline rocks exposed around the city and underlie the alluvial sediments of Quaternary age. The alluvial consists of poorly sorted sand and gravel, clay, and silt in alternating proportions, ranging in thickness from a thin layer to several meters. Al-Madinah is located in a geological depression surrounded by mountains of volcanic and magnetic plutonic rocks. Magnetic plutonic rocks are the basic rocks of the Precambrian Era, whereas volcanic rocks are relatively new. Volcanic rocks in the east and south of Al-Madinah

and sedimentary rocks in the bed of the valley structure two groundwater aquifers, which are linked together **(Fig. 1)**.

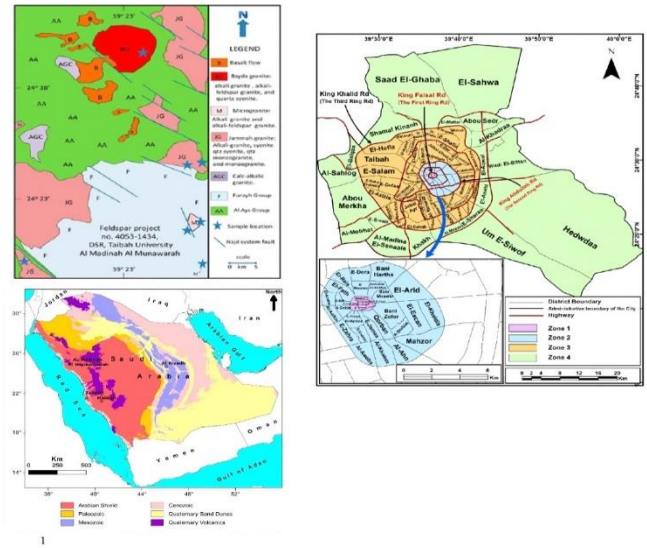

Fig.1: Geological map of Saudi Arabia and Al-Madinah Al-Munawarah area.

Al-Madinah is located in the western province of the Kingdom of Saudi Arabia, 150 km east of the Red Sea and about 400 km north of Makkah **(Fig. 1)**. The city is located at a longitude of 24° 28' N and a latitude of 36° 39' E with a population of 1.10 x 10^6 inhabitants which escalates to more than 1.5 million during the Hajj season. The topography of Al-Madinah comprises plains, hills, and valleys. The ground elevation in the plains varies from 600 to 620 m above mean sea level (amsl). Al Haram, which is located at the center of the city, is about 600 m (amsl). The city is surrounded by mountains from the north, south, and west of the city, ranging in elevation from 800 to 1500 m amsl, with Al Waira mountain being the highest, followed by Uhud (1087 m). The area slopes from east to west until it reaches Al-aqiq valley, and then it slopes from south to north **[**27**]**.

3. Results and discussion

3.1. Radionuclide Concentrations

^{238}U activity concentrations varied between 9.6±0.1 and 15.4±0.6 Bq kg^{-1}, whereas the concentrations of ^{232}Th in the samples, between 6.3±0.5 and 7.9±0.4 Bq kg^{-1}. The activity concentrations of 226Ra ranged between 6.2±0.6 and 8.3±0.4 Bq kg^{-1}. On the other hand, the values of 40K activity concentrations were comparatively varied between 169.3±2.3 and 343.5±1.8 Bq kg^{-1} **(Table 1)**. The activity of ^{40}K is always the major contributor to the specific activity compared with ^{232}Th and 226Ra in all the selected soil samples. The use of chemical fertilizers or changes in the geological and geographical circumstances may be responsible for variations in the radioelement contents in the soil samples under study. The average values for the activity concentrations of ^{226}Ra, ^{232}Th, and 40K across the globe are 32, 45, and 420 Bq kg^{-1}, respectively [1]. The studied soil radionuclide contents were lower than the international limits, suggesting their safe use. By conversion of the activity concentrations from Bq kg^{-1} to ppm, ^{238}U, ^{232}Th, and ^{40}K are varied between 0.77 and 1.05 ppm, 1.55 and 1.95 ppm, and 7.4 and 10.6 wt.%, respectively **(Table 2)**. The relation between the concentration of ^{238}U and ^{232}Th **(Figure 2)** shows that there is a weak or no correlation between them. This may be related to their incorporation in discrete minerals or to uranium migration out concerning thorium due to the prevailing oxidizing conditions. Also, the Th-U intercept exhibits the impoverishment of the Th/U ratio in correlation with the average of continental crust levels.

The correlations between ^{232}Th activity concentrations and ^{238}U activity concentrations derived from the slope in Figure 2 were 0.0112, which is lower than the global ratio of 0.3. The ratio of thorium to uranium, Th/U is one of the most important indicators of soil pollution. Regardless of the origins of the soils, the vast majority of soils in various locations, countries, and regions have a Th/U ratio of 3.5. [28]. The result of our study showed that the Th/U ratio in soils and bottom sediments was lower than 3.5, indicating enrichment of uranium **(Table 2 and Figure 2)**. If this ratio is less than 3.5, that means uranium enrichment **(Figure 3)**, whereas uranium migrates out (depletion of U), is indicated by a higher ratio of more than 3.5 **[**29**]**. ^{232}Th/^{238}U relationship with both ^{238}U and ^{232}Th confirms the previous results **(Figures 3b and 3c)**. The potassium-thorium cross plot is widely used to recognize clay mineral associations and to discriminate micas and feldspars. Furthermore, we noticed a weak correlation between ^{40}K and ^{232}Th activity concentrations with r = 0.04 **(Figure 2)**. Thorium, through adsorption and potassium, through chemical composition, is both associated with clay minerals, making the ratio Th/K a diagnostic marker of other radioactive minerals, where U and Th clarify migration-associated alteration processes **(Figures 3d, 3e, and 3f) [**30**]**. **Table 1** presents the results in which the Th/K ratio ranged between 0.17 and 0.30. These values are much higher than 2×10^{-4}, which indicates that these soil samples are fresh.

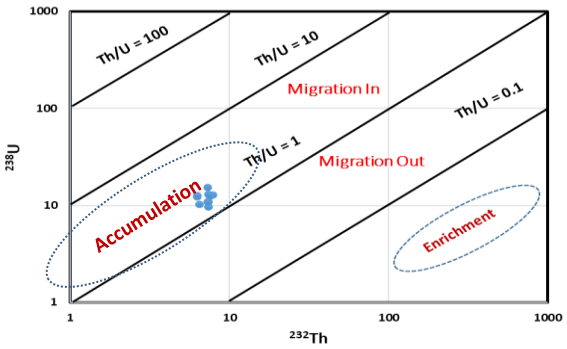

Fig. 2: The distribution of the concentration of Th and U relative to their ratio in soils.

by rainwater, and ii) Recoil energy transfer of a ^{234}U precursor. Moreover, ^{234}Th could be removed from the

Table 1. Radionuclide activity concentrations in the collected soil samples.

Nuclides	1	2	3	4	5	6	7	8	9	10
^{238}U Series										
^{234m}Pa	10.1±0.2	11.4±0.1	12.3±0.2	9.7±0.08	10.7±0.1	16.5±0.6	9.6±0.4	13.2±0.5	15.4±0.2	13.5±0.2
^{234}Th	10.4±0.1	12.9±0.09	13.1±0.1	11.9±0.09	8.5±0.1	14.3±0.5	12.2±0.5	12.5±0.9	9.5±0.4	12.5±0.4
Average	10.3±0.1	12.2±0.1	12.7±0.3	10.8±0.09	9.6±0.1	15.4±0.6	10.9±0.5	12.9±0.7	12.5±0.3	13±0.3
^{234}U	18.9±1.4	15.3±0.8	16.2±0.7	15.2±0.9	16.4±0.7	14.3±0.4	15.2±0.9	17.1±0.6	15.2±0.7	16.3±0.7
^{230}Th	8.4±0.2	9.1±0.8	9.4±0.2	8.4±0.7	10.1±0.6	8.4±0.3	9.6±0.6	10.4±0.9	8.6±0.3	7.9±0.6
^{226}Ra	7.4±0.4	6.2±0.6	7.6±0.4	7.5±0.4	7.3±0.4	7.2±0.9	7.6±0.5	7.4±0.9	8.3±0.4	7.6±0.2
^{214}Pb	6.7±0.1	7.4±0.2	8.2±0.7	8.4±0.3	6.4±0.3	7.2±0.2	7.4±0.5	7.6±0.3	7.1±0.2	7.3±0.1
^{214}Bi	6.7±0.1	7.4±0.3	7.4±0.3	7.2±0.6	7.3±0.4	7.4±0.8	7.5±0.5	8.4±0.4	7.9±0.6	7.9±0.9
^{232}Th Series										
^{228}Ac	6.1±0.5	6.2±0.4	6.4±0.6	7.4±0.5	7.3±0.2	8.2±0.9	7.6±0.3	7.3±0.6	7.5±0.3	7.2±0.3
^{208}Tl	6.9±0.2	6.4±0.5	6.2±0.7	7.3±0.4	7.5±0.2	6.4±0.2	6.9±0.9	8.4±0.2	7.4±0.3	7.5±0.9
Average	6.5±0.4	6.3±0.5	6.3±0.7	7.4±0.5	7.4±0.2	7.3±0.6	7.3±0.6	7.9±0.4	7.5±0.3	7.4±0.6
^{235}U	0.47±0.01	0.56±0.01	0.58±0.01	0.50±0.01	0.44±0.01	0.71±0.02	0.51±0.02	0.58±0.01	0.57±0.06	0.57±0.09
^{40}K	262.9±1.3	169.3±2.3	301.3±1.2	256.5±1.8	251.2±2.1	238.9±1.7	246.5±2.1	240.9±1.9	343.5±1.8	246.5±1.9
^{238}U/ ^{235}U	21.9±0.7	21.8±0.6	21.9±0.9	21.6±0.6	21.8±0.7	21.7±1.5	21.4±1.8	22.2±1.6	21.9±2.8	22.8±4.1
^{234}U/ ^{235}U	40.2±3.8	27.3±1.9	27.9±1.7	30.4±2.4	37.3±2.4	20.1±1.1	29.8±2.9	29.5±1.5	26.7±4	28.6±5.7
^{234}U/ ^{238}U	1.83±0.15	1.25±0.08	1.28±0.09	1.41±0.1	1.71±0.09	0.93±0.06	1.39±0.15	1.33±0.12	1.22±0.09	1.25±0.08
^{238}U/ ^{234}U	0.5±0.01	0.8±0.01	0.8±0.02	0.7±0.01	0.6±0.01	1.1±0.01	0.7±0.01	0.8±0.01	0.8±0.01	0.8±0.01
^{226}Ra/ ^{238}U	0.72±0.05	0.51±0.05	0.6±0.05	0.69±0.04	0.76±0.05	0.47±0.08	0.70±0.08	0.57±0.1	0.66±0.05	0.58±0.04
^{230}Th/ ^{238}U	0.82±0.03	0.75±0.07	0.74±0.03	0.78±0.07	1.05±0.07	0.55±0.04	0.88±0.1	0.81±0.11	0.69±0.04	0.6±0.06
^{226}Ra/ ^{230}Th	0.88±0.07	0.68±0.13	0.81±0.06	0.89±0.12	0.72±0.08	0.86±0.14	0.79±0.1	0.71±0.15	0.97±0.08	0.96±0.12
^{230}Th/ ^{234}U	0.40±0.04	0.60±0.08	0.60±0.04	0.60±0.08	0.60±0.06	0.59±0.04	0.63±0.08	0.61±0.07	0.57±0.05	0.48±0.06

3.2. Uranium Series Isotopic Ratios

$^{234}U/^{238}U$ activity ratios in most soil samples are greater than unity from1.22±0.09 to1.83±0.15 except one sample has value <1 (0.93±0.06) value, indicating relatively recent U uptake and preferential ^{234}U accumulation due to the prevailing reduction conditions (i.e., < 1 Ma) from fluids that carried excess 234U from the adjacent rocks. The difference in $^{234}U/^{238}U$ activity ratio in the studied soil may be related to: i) the selectivity of ^{234}U during leaching grain surface to the water by alpha recoil transfer and decays to 234U, which remains soluble [31].

The difference in the $^{234}U/^{238}U$ activity ratio in the studied soil may be connected to the reduction or oxidation conditions. The difference in the $^{230}Th/^{234}U$ activity ratio could be related to the variation in the chemical properties of ^{230}Th and ^{234}U due to α-decay enhanced dissolution, re-adsorption, and re-precipitation of ^{234}U. The disequilibrium of $^{226}Ra/^{230}Th$ can be ascribed to the complexation of

thorium with Cl^- and SO_4^{2-} and to the co-precipitation of radium with sulfates resulting from Phosphogypsum fertilizer and rainwater. A significant difference in the $^{238}U/^{235}U$ ratio in the soil samples, 21.4±1.8 and 22.8±4.1, suggested that redox plays an important role in the fractionation of ^{238}U and ^{235}U **[**32, 33, 34, and 35**]**.

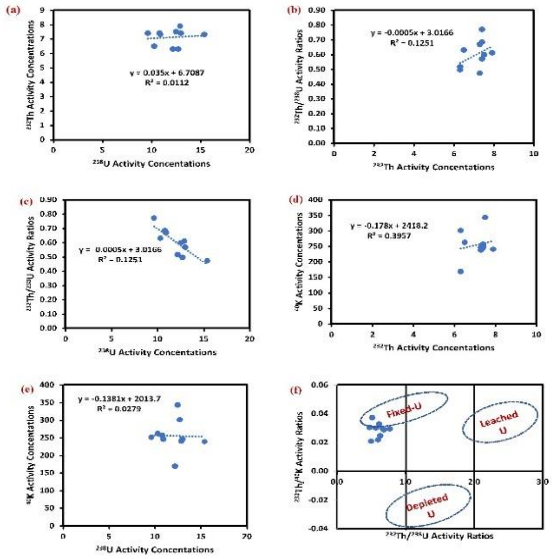

Fig.3: a) ^{238}U vs ^{232}Th, b) ^{232}Th vs $^{232}Th/^{238}U$, c) ^{238}U vs $^{232}Th/^{238}U$, d) ^{232}Th vs ^{40}K, e) ^{238}U-^{40}K, f) $^{232}Th/^{238}U$ vs $^{232}Th/^{40}K$ in the studied soil samples.

A technique for tracking the migration of radionuclides from the uranium series in various environments is the ratio of U to Th isotope activity **(Table 2, Figure 4)**. In contrast to locations of primordial ^{238}U, ^{234}U is produced via alpha decay and, as a result, inhabits a radiation-damaged site that is more prone to leaching. Due to the loss of electrons during ^{238}U's decay, the ^{234}U is also likely to be oxidized to U^{VI}, making it more soluble than the parent ^{238}U, which often occurs in primary minerals as the reduced and less soluble U^{IV}. The alpha-recoil effect, which occurs on grain surfaces, is a third mechanism that increases the mobility of U [36].

Plotting the activity ratios of $^{234}U/^{238}U$ versus $^{230}Th/^{238}U$ [37] of the studied soil samples indicated the variation of these ratios ($^{234}U/^{238}U$ and $^{230}Th/^{238}U$) from secular equilibrium. Most of the studied samples lie in the reduction zone (accumulation zone), which represents the zone of uranium accumulation, suggesting that the prevailing reduction conditions, which may be connected with using phosphogypsum as fertilizer or the abundance of sulphide in it. Only two samples are plotted in the forbidden zone, suggesting fluctuation in the physico-chemical conditions, which may be connected to the effect of acidic water. Also, these ratios indicated a recent migration of ^{228}Ra (^{228}Th) from the studied soil samples by the effect of hydro-chemical characteristics of underground or surficial water **(Figure 4)**.

Table. 2. Radionuclide concentrations of ^{238}U, ^{232}Th, and ^{40}K in ppm for the collected Soil sampl

Samples	^{238}U ppm	^{232}Th ppm	^{40}K ppm	U/Th	Th/U	Th/K	K/U	U-Th/3.5
1	0.83	1.6	8.1	0.52	1.93	0.19	9.8	-0.22
2	0.98	1.55	5.2	0.63	1.58	0.30	5.3	-0.16
3	1.02	1.55	9.3	0.66	1.52	0.17	9.1	-0.15
4	0.87	1.82	7.9	0.48	2.09	0.23	9.1	-0.27
5	0.77	1.82	7.8	0.42	2.35	0.23	10.1	-0.30
6	1.24	1.8	7.4	0.69	1.45	0.24	5.9	-0.16
7	0.88	1.8	7.6	0.49	2.05	0.24	8.6	-0.26
8	1.04	1.95	7.4	0.53	1.87	0.26	7.1	-0.26
9	1.01	1.85	10.6	0.55	1.83	0.17	10.5	-0.24
10	1.05	1.82	7.6	0.58	1.74	0.24	7.2	-0.22

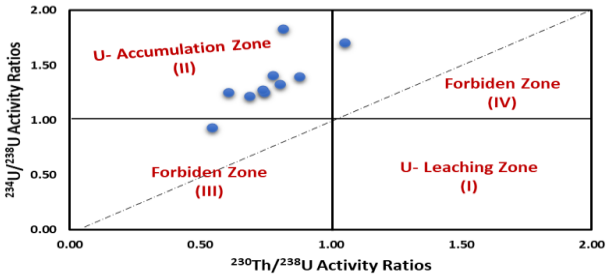

Fig. 4: $^{234}U/^{238}U$ versus $^{230}Th/^{238}U$ (Thiel diagram) of the studied soil samples.

Table 3: Environmental Hazard Impacts Calculations for the studied soil samples.

Ra_{eq}	Absorbed Gamma Dose Rate (AGDR)	Annual Effective Dose Rate	H_{ex}	H_{in}	Gamma Index (I_γ)	ELCR
35.03	116.30	0.14	0.10	0.12	0.29	0.47
27.00	76.87	0.09	0.08	0.09	0.22	0.31
37.64	132.17	0.16	0.11	0.13	0.31	0.54
35.96	114.26	0.14	0.10	0.12	0.30	0.46
35.39	111.97	0.14	0.10	0.12	0.29	0.45
34.29	106.77	0.13	0.10	0.12	0.28	0.43
35.22	110.10	0.14	0.10	0.12	0.29	0.45
35.48	108.07	0.13	0.10	0.12	0.29	0.44
43.00	150.71	0.18	0.12	0.15	0.36	0.61
35.36	110.16	0.14	0.10	0.12	0.29	0.45
27.00	76.87	0.09	0.08	0.09	0.22	0.31
43.00	150.71	0.18	0.12	0.15	0.36	0.61
35.44	113.74	0.14	0.10	0.12	0.29	0.46

3.3. Environmental Hazard Impacts

Absorbed dose rate (ADR compliance aids in the avoidance of deterministic effects and the control of

potential stochastic impacts. All values were clearly above the permissible limit, 55 nGy h^{-1}. The values of absorbed gamma dose rate, AGDR was ranged between 76.87 and 150.71 nGy h^{-1} with an average value of 113.74 nGy h^{-1} **(Table 3).** It is worth mentioning that the collected granite samples exceed the permissible levels due to the presence of radioelement-bearing minerals such as zircon and monazite. The annual effective dose rate values in the collected samples ranged between 0.09 and 0.18 mSv y^{-1}, with an average of 0.14 mSv.y-1 **(Table 3)**. All the collected samples were higher than the permissible limit of the annual effective dose rate, 0.48 mSv y^{-1} **[**38**]**. Radium equivalent values are widely used to identify the consistency of radiation exposure. It is related to both the external γ-dose and the internal α-dose from radon and its progeny. Raeq values for all studied samples were computed and are listed in **Table 2**. They fluctuated between 27 and 43 Bq kg^{-1}, with an average value of 35.44 Bq kg^{-1}, which is lower than the recommended limit of 370 Bq kg^{-1} **(Table 3)**.

For the safe utilization of granitic rocks as building materials, H_{ex} and H_{in} ought not to be above unity [39]. H_{ex} values ranged between 0.08 and 0.12, with an average value of 0.10 **(Table 2)**, which falls lower than the permissible limit (unity); these results point to the fact that the collected rocks aren't harmful and are safe to be used. The internal hazard index, H_{in}, gives the internal exposure to carcinogenic radon and its short-lived progeny. Paradoxically, H_{in} values ranged between 0.09 and 0.15, with an average value of 0.12 falling below unity **(Table 3).** The gamma index (I_γ) was calculated to see if our granitic samples meet those two standards. Materials for the decorative surface and other building uses, such as tiles, boards, and granite, meet the dose requirement for exemption, 0.3 mSv y^{-1}, while the dose criterion of 1 mSv y^{-1} conforms to an $I_\gamma > 6$ gamma representative level index. However, because these values correspond to annual effective dose rates greater than 1 $mSvy^{-1}$ **[**38**]**. Samples with $I_\gamma > 6$ cannot be used in construction. The studied granite samples' gamma index (I_γ) values were calculated. The average value was 6.04, with a range of 0.7 to 12.8 **(Table 3)**. Annual gonadal equivalent dose values in the collected samples ranged between 98.65 and 164.86 mSv y^{-1} with an average of 133.01 mSv y^{-1}.

AGED value is much lower than the world average values for soil, 0.298 mSv y^{-1}. Results presented in **Table 2** indicated that the commonly used building materials, which are examined in this work, could be used in building construction without exceeding the proposed radioactivity criterion level. Thus, by using such building materials, buildings could work as shields for residents against terrestrial radiation. The investigated dendrogram is tabulated in **Figure 4**, showing three clusters. Cluster-I includes ^{238}U, ^{226}Ra with ED, H_{ex}, H_{in}, I_γ, and Absorbed Dose (AD. Uranium was found to be closely grouped with all the hazard indices: Ra_{eq}, D_{air}, AED_{in}, AED_{out}, H_{ex}, H_{in}, I_γ, AGDE, and ELCR, indicating a notable degree of similarity and variance among these indices. In contrast, ^{232}Th and ^{40}K were identified in a separate cluster, positioned at a considerably greater linkage distance from the uranium cluster. This suggests that the impact of these radionuclides on radiological exposure levels is generally less significant than that of uranium, thereby indicating their relatively minor role compared to uranium. Furthermore, the Hierarchical Cluster Analysis (HCA) corroborates the results obtained from the Pearson correlation analysis, offering evidence that variations in radiological hazard across the samples are predominantly attributable to uranium enrichment, with ^{232}Th and ^{40}K contributing only in lesser quantities **(Figure 5)**. This may indicate that the main environmental health hazard parameters exist due to the activity concentrations of ^{238}U and ^{226}Ra. Cluster-II contains ^{232}Th and Ra_{eq}. Cluster III consists only of ^{40}K, which illustrates that the activity concentration of potassium doesn't contribute to the natural radioactivity **(Figures 5 and 6)**.

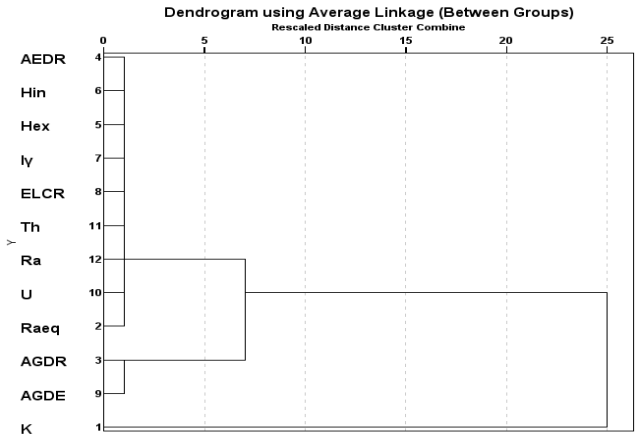

Fig.5:Linkage between the samples under study of various statistical radiological hazard indexes.

The PCA results presented in **Figure 6** indicate that components 1 and 2 account for more than 95% of the total variance. Component 1 is primarily influenced by radiological hazard indices (Ra_{eq}, D_{air}, $AGDE_{in}$, AEDR, H_{ex}, H_{in}, I_γ, ELCR, and AGDR), which exhibit strong loadings and positive correlations, suggesting a significant interrelationship among these parameters and indicating that these indices are interconnected. The strong correlation with ^{238}U suggests that uranium is the key factor influencing radiological risk in the current black shale. In contrast, ^{232}Th and ^{40}K show a weaker and more independent association, with lower loadings relative to the uranium-hazard cluster. On component 2, which further distinguishes the hazard index and uranium from other variables, the ELCR variable is associated with the hazard indices along component 1. This indicates that ELCR is significantly influenced by the

overall radiation dose. In conclusion, the PCA findings highlight that uranium plays a crucial role in radiological impacts, while thorium and potassium are of lesser importance **(Figure 6)**.

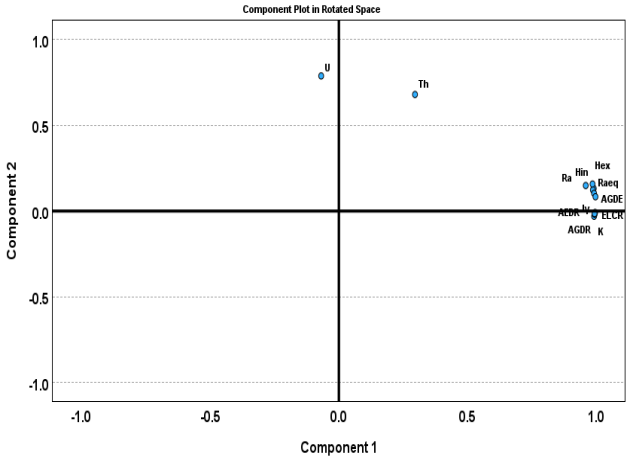

Fig. 6: Principal component analysis (PCA) of ^{238}U, ^{232}Th, and ^{40}K activity concentrations with radiological hazard indices in the black shale samples.

4. Conclusion

^{238}U activity concentrations varied from 9.6±0.1 to 15.4±0.6 Bq kg^{-1}, ^{232}Th between 6.3±0.5 to 7.9±0.4 Bq kg^{-1}, ^{226}Ra between 6.2±0.6 and 8.3±0.4 Bq kg^{-1} and ^{40}K between 169.3±2.3 and 343.5±1.8 Bq kg^{-1}. The studied soil radionuclide contents are lower than the international limits, suggesting their safe use.

The Th/U ratio in soils and bottom sediments is lower than 3.5, indicating enrichment of uranium. ^{234}U/^{238}U and ^{230}Th/^{238}U activity ratios showed that most soil samples lie in the accumulation zone, except for two samples in the forbidden zone, suggesting the prevailing reduction conditions. ^{234}U/^{238}U activity ratio in most soil samples was greater than unity, indicating relatively recent U uptake and preferential ^{234}U accumulation. The difference in ^{230}Th/^{234}U activity ratio could be related to the variation in the chemical properties of uranium and thorium, in addition to α-decay enhanced dissolution, re-adsorption, and re-precipitation of ^{234}U. All the calculated environmental hazard parameters of the soil samples are within the range of international levels, confirming their safe use. The cluster analysis exhibits that the main environmental health hazard parameters exist due to the activity concentrations of ^{238}U and ^{226}Ra.

References

[1] UNSCEAR. 2010. United National Scientific Committee on the Effects of Atomic Radiation. Sources and Effects of Ionizing Radiation: Report to the General Assembly, with Scientific Annexes Vol. 1. United Nations, 1-219. https://doi.org/10.18356/a02938bf-en.

[2] Madkour, HA., Mansour, AM ., Ahmed, AEHN., El-Taher, A., 2014 Environmental texture and geochemistry of the sediments of a subtropical mangrove ecosystem and surrounding areas, Red Sea Coast, Egypt. Arabian Journal of Geosciences 7 (9), 3427-3440.

[3] El-Taher, A., Althoyaib, S.S. 2012. Natural radioactivity levels and heavy metals in chemical and organic fertilizers used in the Kingdom of Saudi Arabia. Applied Radiation and Isotopes, 70, 290-295, https://doi.org/10.1016/j.apradiso.2011.08.010.

[4] Osmond, K., Ivanovich, M. 1992. Uranium-series mobilization and surface hydrology. In: Ivanovich, M., Harmon, R.S. (Eds.), Uranium Series Disequilibrium: Application to Earth, Marine, and Environmental Sciences. Oxford Sciences Publications, Oxford. 259-289.

[5] Anjos, R.M., Veiga, R., Soares, T., Santos, A., Aguiar, J.G., Frascá, M., Brage, J., Uzêda, D., Mangia, L., Facure, A., Mosquera, B., Carvalho, C., Gomes, P. 2005. Natural radionuclide distribution in Brazilian commercial granites. Radiat. Meas. 39, 245-253.

[6] Gilmore, G.R. 2008. Practical Gamma-ray Spectroscopy. 2nd ed., John Wiley & Sons, Ltd., p. 408.

[7] Kalintsev, A., Migdisov, A., Alcorn, C. et al. 2021. Uranium carbonate complexes demonstrate a drastic decrease in stability at elevated temperatures. Commun Chem 4, 120. https://doi.org/10.1038/s42004-021-00558-3.

[8] Amini Birami, F., Moore, F., Faghihi, R., Keshavarzi, B. 2019. Distribution of natural radionuclides and assessment of the associated radiological hazards in the rock and soil samples from a high-level natural radiation area, Northern Iran. J. Radioanal. Nucl. Chem. 322, 2091-2103, https://doi.org/10.1007/s10967-019-06912-z.

[9] El Galy, M.M., El Mezayn, A.M., Said, A.F., El Mowafy, A.A., Mohamed, M.S. 2008. Distribution and environmental impacts of some radionuclides in sedimentary rocks at Wadi Naseib area, southwest Sinai, Egypt. J. Environ. Radioact. 99, 1075-1082.

[10] Adagunodo, T.A., Sunmonu, L.A., Adabanija, M.A., Omeje, M., Odetunmibi, O.A., Ijeh, V. 2019. Statistical assessment of radiation exposure risks of farmers in Odo Oba, Southwestern Nigeria. Bull. Min. Res. Exp. 159, 201-217.

[11] Pan, Z., Roebbert, Y., Beck, A., Bartova, B., Vitova, T., Weyer, S., Bernier-Latmani, R. 2022. Persistence of the Isotopic Signature of Pentavalent Uranium in Magnetite. Environ. Sci. Technol. 56, 1753-1762.

[12] Abuelnaga, H.S.O., Harbi, H. M., Alqahtani, F. A., Bamousa, A. O. M., Aboud, E. 2021. Radiological environmental studies of Al Aziziah area and vicinity, Al Madinah Al Monawarah, Saudi Arabia. Environ. Monit. Assess. 193, 87.

https://doi.org/10.1007/s10661-021-08883-9.

[13] Fallatah, O., Khattab, M.R. 2023. Evaluation of environmental radioactivity and hazard impacts of Saudi Arabian granitic rocks used as building Materials. Minerals. 13, 165. https://doi.org/10.3390/min13020165.

[14] A. El-Taher, WM Badawy, AEM Khater, HA Madkour., 2019 Distribution patterns of natural radionuclides and rare earth elements in marine sediments from the Red Sea, Egypt. Applied Radiation and Isotopes 151, 171-181.

[15] Madkour, H.A., El-Taher, A., Ahmed, A.N., Mohamed, A.W., El-Erian, T.M., 2012. Contamination of Coastal Sediments in El-Hamrawein Harbour, Red Sea, Egypt. J. Environ. Sci. Tech. 5, 210-221.

[16] Khattab, M.R. 2022. Using uranium and thorium isotopes in age framework determination for different stages of alterations and mineralization in Missikat altered granites, Central Eastern Desert, Egypt. Phys. Chem. Earth. 128, 103204.

[17] Elsaman, R., Seleem, EMM., Salman, SA., Ella, EMAE., El-Taher, A., 2022 Evaluation of natural radioactivity levels and associated radiological risk in soil from Siwa Oasis, Egypt. Radiochemistry 64 (3), 409-415.

[18] Kinsara, A.A., Shabana, E.I., Qutub, M.M.T. 2014. Natural Radioactivity in Some Building Materials Originating from a High Background Radiation Area. Int. J. Innovat. Edu. Res. 2, 70-78.

[19] Arafin, SAK., El-Taher, A., Hoque, AKMF., Hoque, MA., Ferdous, J., Abedin, MJ., 2020 Natural gamma radiation level detection in agricultural soil after Aila disaster and comparison with deep soil gamma activity in a specific area of Sundarban region, Satkhira, Bangladesh International Journal of Radiation Research 18 (3), 397-404

[20] Güna, O. 2018. Assessment of lifetime cancer risk from natural radioactivity levels in Kadikoy and Uskudar District of Istanbul. Arab. J. Geosci. 11, 782.

[21] Abdel Gawad, AE., Ghoneim, MM., El-Taher, A., Ramadan, AA., 2021 Mineral chemistry aspects of U-, Th-, REE-, Cu-bearing minerals at El-Regeita shear zone, South Central Sinai, Egypt. Arabian Journal of Geosciences 14 (14), 1356.

[22] Laissaoui, A., Mejjad, N., Ziad, N., Ait, B.H., El Hammoumi, O., Benkdad, A., Fekri, A. 2018. Evidence for a recent increase in delivery of atmospheric 210Pb to Oualidia lagoon, coastal Morocco. Environ Monit Assess 190, 642. http://doi.org/10.1007/s10661-018-7046-z.

[23] Sharaf, J.M., Hamideen, M.S. 2013. Measurement of natural radioactivity in Jordanian building materials and their contribution to the public indoor gamma dose rate, Applied Radiation and Isotopes, 80, 61-66, https://doi.org/10.1016/j.apradiso.2013.06.016.

[24] Ahmed, A., Burdin, S., Casse, G., Van Zalinge, H., Powell, S., Rees, J., Smith, A., Tsurin, I. 2016. GAMBE: multipurpose sandwich detector for neutrons and photons. Radiation Detectors: Systems and Applications XVII 9969, 59-67.

[25] Abdel-Rahman, M.A.E., Sabry, M., Khattab, M.R., El-Taher, A., El Mongy, S.A. 2020. Radioactivity and Risk Assessment with Uncertainty Treatment for Analysis of Black Sand Minerals. ZAAC. https://doi.org/10.1002/zaac.202000176.

[26] Mamont-Ciesla, K., Gwiazdowski, B., Biernacka, M., Zak, A. 1982. Radioactivity of building materials in Poland. In: G. Vohra, K.C. Pillai and S. Sadavisan (Eds.) Natural Radiation Environment Halsted Press, New York, 551.

[27] Gutub, S.A. et al., 2004. A Feasibility Study of Groundwater and its Usage in the Central Area in Al-Madinah Al-Munawara, Report Zuhair Fayez Partnership Consultants.

[28] Rikhvanov, L.P., Arbuzov, S.I., Baranovskaya, N.V., Volostnov, A.V., Arkhangelskaya, T.A., Mazhibor, A.M., Berchuk, V.V., Zhornyak, L.V., Zamyatina, Y.L., Ivanov, A.Y., Talovskaya, A.V., Shatilova, S.S., Yazikov, E.G. 2007. Radioactive Elements in the Environment. News of Tomsk Polytechnic University 311, 128-136. https://elibrary.ru/download/elibrary_11676076_51224496.pdf

[29] Chabaux, F., Granet, M. E., Pelt, E., France-Lanord, CV. Galy, V. 2006. ^{238}U-^{234}U-^{230}Th disequilibria and timescale of sedimentary transfers in rivers: Clues from the Gangetic plain rivers, Journal of Geochemical Exploration, 88, 373-375, https://doi.org/10.1016/j.gexplo.2005.08.078.

[30] Fallatah O, Khattab MR. 2023. Evaluation of Environmental Radioactivity and Hazard Impacts Saudi Arabia Granitic Rocks Used as Building Materials. Minerals. 13 (2):165. https://doi.org/10.3390/min13020165.

[31] Papadopoulos, A., Christofides, G., Koroneos, A., Papadopoulou, L., Papastefanou, C., Stoulos, S. 2013. Natural radioactivity and radiation index of the major plutonic bodies in Greece. J. Environ. Radioact. 124, 227-238.

[32] S. Weyer, S., Anbar, A.D., Gerdes, A., Gordon, G.W., Algeo, T.J., Boyle, E.A. 2008. Natural fractionation of 238U/235U, Geochimica et Cosmochimica Acta, 72, 345-359, https://doi.org/10.1016/j.gca.2007.11.012.

[33] Montoya-Pino, C., Weyer, S., Anbar, A.D., Pross, J., Oschmann, W., Schootbrugge, Bvd., Helge, W.A. 2010. Global enhancement of ocean anoxia during Oceanic Anoxic Event 2: a quantitative approach using U isotopes. Geol. 38, 315-318.

[34] El-Feky, M.G., Mohammed, H.S., El-Shabasy, A.M., Ahmed, M.R., Abdel-Monem, Y.K., Mira, H.I. 2021. Mobilization of radionuclides during uranium and gold processing of granitic rock at El-Missikat area, central Eastern Desert, Egypt. Int. J. Environ. Anal. Chem.

https://doi.org/10.1080/03067319.2021.1925262.

[35] Khattab, M.R., Tuovinen, H., Lehto, J., El Assay, I.E., El Feky, M.G., Abd El-Rahman, M.A. 2017. Determination of uranium in Egyptian granitic ore by gamma, alpha, and mass spectrometry. Instrum. Sci. Technol. 45, 338-348.

[36] Gascoyne, M., Millera, N.H., Neymarkb, L.A. 2002. Uranium-series disequilibrium in tuffs from Yucca Mountain, Nevada, as evidence of pore-fluid flow over the last million years. Appl. Geochem. 17, 781. https://doi.org/10.1016/S0883-2927(02)00038-0.

[37] Thiel, K., Saager, R., Muff., R. 1980. U-fission track micromapping as a means to study uranium mobilization processes in Precambrian sediments, Nuclear Instruments and Methods, 173, 223-227, https://doi.org/10.1016/0029-554X(80)90592-3.

[38] Mabrouk, S., Abd El Monsef, M., Abart, R., Toksoy-Köksal, F., Abdelfadil, K.M. 2022. Unraveling the Genesis of Highly Fractionated Rare-Metal Granites in the Nubian Shield via the Rare-Earth Elements Tetrad Effect, Sr-Nd Isotope Systematics, and Mineral Chemistry. ACS. Earth. Space. Chem. 6, 2368-2384.

[39] Oraby, AH., Saleh, GM., Hassan, EM., Eldabour, SE., El Tohamy, AM., Kamar, MS., El Feky, MG., El Taher, A., (2022) Natural radioactivity and radioelement potentiality of mylonite rocks in Nugrus Area, Southeastern Desert, Egypt. Radiochemistry 64 (5), 645-655.